Input Impedance of a Probe-Excited Semi-Infinite Rectangular Waveguide with Arbitrary Multilayered Loads: Part II—A Full-Wave Analysis

Le-Wei Li, *Senior Member, IEEE,* Pang-Shyan Kooi, *Member, IEEE,* Mook-Seng Leong, *Member, IEEE,* Tat-Soon Yeo, *Senior Member, IEEE,* and See-Loke Ho

***Abstract*— Utilizing the dyadic Green's functions (DGF's) derived in Part I of this paper, the input impedance of a coaxial probe located inside a semi-infinite rectangular waveguide has been generally formulated. The electromagnetic DGF's for a rectangular cavity with a dielectric load are also obtained from the general expressions given in Part I. Using the full-wave analysis, a dielectric-loaded rectangular cavity is further considered and the input impedance is specified. To improve the computational accuracy, an alternative form of electric DGF's of the second kind is developed and expressed in terms of the guided-wave eigenvalues for the rectangular loaded cavity. The probe-input reactance and the phase of the reflection coefficients are computed using the conventional form of electric DGF and the alternative form of magnetic DGF. Data are obtained from experiments performed on a dielectric-loaded cavity and compared with the numerical results. Agreement of the theoretical and experimental results confirms the applicability of the theoretical analysis given in this paper.**

I. Introduction

THE INPUT impedance of a probe is of particular importance to the microwave component designers [1]–[4]. For the determination of the input impedance of a coaxial probe inside a rectangular waveguide, the Method of Moments (MoM's) and the dyadic Green's function (DGF) technique are usually applied [5]–[8]. Some simple geometries such as an empty rectangular cavity [7], [9], and [10], an empty rectangular semi-infinite waveguide [5], and a dielectric-loaded semi-infinite waveguide [6] have been dealt with using these methods. However, the conventional form of the magnetic DGF consists of the singularity and the step-functional sign change which reduce the computational speed for a given accuracy or introduce error for a given number of iteration [9]. It has recently been found [10] that the use of an alternative form of the magnetic DGF can improve computational speed and accuracy. Also, it is helpful for system design if further investigations on the input impedance of a coaxial probe located in complex structures are conducted.

This paper aims at determining the input impedance of a coaxial probe in a semi-infinite rectangular waveguide with multiple *loads* by using the electric DGF's presented in [8] and an alternative form of magnetic DGF's. The input impedance of a probe inside a dielectric-loaded rectangular cavity, as an application, has been analyzed. The problem of the input impedance of a probe located in a rectangular waveguide with multiple loads is first stated in Section II. A practical case of a dielectric-loaded rectangular cavity, which can be considered as a specific structure of the semi-infinite rectangular waveguide with a dielectric and a conducting loads, is then discussed in Section III. Electromagnetic DGF's of the first kind for the semi-infinite rectangular waveguide are directly reduced in Appendix A from the general formulae given in [8]. For ease of numerical implementation, the alternative form of the electric DGF of the second kind is represented in Appendix B. Probe-input impedance is computed using the MoM's and the alternative DGF form. To verify the theoretical analysis, comparison is made between experimental data and computed results. Reasonably good agreements of the theoretical and experimental results are found from the comparison in Section III.

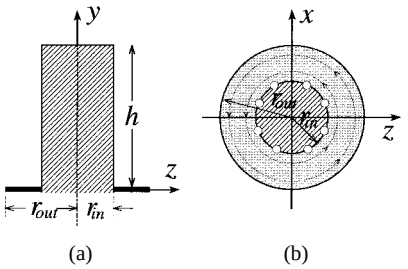

Fig. 1. (a) Side view and (b) top view of the excited probe. The equivalent surface current flowing circularly over the disk plate forms the magnetic source.

II. Statement and Formulation of the Problem

To formulate the problem, the structure of the waveguide and the representation of the source probe are described first. The calculation of the probe-input impedance using the MoM's is given subsequently.

A. Source Representation and Waveguide Structure

In this problem, a semi-infinite rectangular waveguide with multiple loads is excited by a coaxial probe of characteristic impedance Z_0 (in experiments, a 50-Ω impedance is chosen). See Fig. 1 for geometry of the probe.

Manuscript received June 11, 1995; revised November 21, 1996.

The authors are with the Department of Electrical Engineering, Communications and Microwave Division, National University of Singapore, Singapore 119260.

Publisher Item Identifier S 0018-9480(97)01708-0.

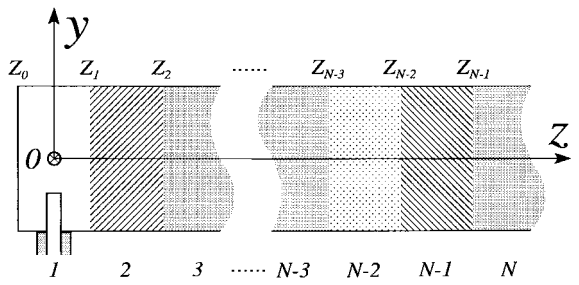

Fig. 2. Geometry of the semi-infinite rectangular waveguide with multiple loads.

The probe itself is usually considered as an electric source. A sinusoidal filamentary current distribution is assumed along the entire length of the probe situated at the center. The first edition of [1], as well as [2], [11], and [12], used this assumption to investigate the probe radiation inside a rectangular waveguide. Due to the electromagnetic scattering from the cylindrical post inside the waveguide, the probe surface current is not uniformly distributed around the probe. Therefore, the probe cannot be accurately represented by just a centered filamentary current. Instead, the metallic probe can be represented as a set of $\hat{\boldsymbol{y}}$-directed current filaments situated along the circumference of the probe. In [5], [13], and [14] eight equivalent current filaments representation are used to replace the conducting-post surface and effectively modified the previous single post with a central current.

When a signal is fed into the coaxial cable, a known magnetic frill current distribution at the base of the coaxial-to-rectangular feed induces an unknown current distribution in the presence of the waveguide walls. The circular current flow on the disk-shaped aperture is equivalent to a magnetic source, as shown in Fig. 1. Thus, for the probe considered (see Fig. 1), the eight equivalent current filaments form the electric-current distribution $\boldsymbol{J}(\boldsymbol{r}')$ of $\hat{\boldsymbol{y}}$-direction and the equivalent current flow along the surface of the frill current aperture forms the magnetic current distribution $\boldsymbol{M}(\boldsymbol{r}')$ of both $\hat{\boldsymbol{x}}$- and $\hat{\boldsymbol{z}}$-directions. Both [6] and [7] included the effects from the frill current due to the probe located in the waveguide and cavity and also derived the expression of the DGF's in component form, respectively. In this paper, the same representation of the probe will be employed in our calculation.

B. Field Equations and Dyadic Green's Functions (DGF's)

The electromagnetic fields excited by the probe in the semi-infinite rectangular waveguide with multiple loads as shown in Fig. 2 are governed by Maxwell's equations. Instead of solving the vector–wave equations directly, the authors solve for the fields using DGF's. In component form, the $\hat{\boldsymbol{y}}$-directed electric fields $\boldsymbol{E}^J_{yi,\,i'}$ and $\boldsymbol{E}^I_{yi}$ at the field point i due to the i'th filamentary electric source $\boldsymbol{J}_e(\boldsymbol{r}')$ and the frill source $\boldsymbol{M}_s(\boldsymbol{r}')$ at the probe base are expressed by

$$\boldsymbol{E}^J_{yi,\,i'} = i\omega\,\mu \iiint_V [\overline{\boldsymbol{G}}_e(\boldsymbol{r},\boldsymbol{r}')]_{yy} J_{ey}(\boldsymbol{r}')\,dV' \tag{1a}$$

$$\boldsymbol{E}^I_{yi} = -\iiint_V [\nabla\times\overline{\boldsymbol{G}}_m(\boldsymbol{r},\boldsymbol{r}')]_{yx} M_{sx}(\boldsymbol{r}')\,dV' - \iiint_V [\nabla\times\overline{\boldsymbol{G}}_m(\boldsymbol{r},\boldsymbol{r}')]_{yz} M_{sz}(\boldsymbol{r}')\,dV'. \tag{1b}$$

It can be seen from (1) that the electric field can be obtained if the electromagnetic DGF's [i.e., $\overline{\boldsymbol{G}}_e(\boldsymbol{r},\boldsymbol{r}')$ and $\overline{\boldsymbol{G}}_m(\boldsymbol{r},\boldsymbol{r}')$] and the electromagnetic sources [i.e., $\boldsymbol{J}_e(\boldsymbol{r}')$ and $\boldsymbol{M}_s(\boldsymbol{r}')$] are known.

In fact, the $\hat{\boldsymbol{y}}$-directed electric-current distribution $\boldsymbol{J}_e(\boldsymbol{r}')$ as a function of y' and ϕ' can be expressed as

$$J_y(y',\,\phi) = \sum_{s'=1}^{2} j_{s',\,t'} t_{s'}(y') p_{i'}(\phi') \tag{2a}$$

and

$$\boldsymbol{M}_s(\boldsymbol{r}') = \frac{V_0}{r'\,\ln\left(\dfrac{r_{\text{out}}}{r_{\text{in}}}\right)}\,(-\cos\phi'\hat{\boldsymbol{x}} + \sin\phi'\hat{\boldsymbol{z}}) \tag{2b}$$

where V_0 is the coaxial input voltage at $y=-b/2$, b is the height of the rectangular waveguide, $j_{s',\,t'}$ are the unknown coefficients, $t_{s'}(y')$ are the following expansion (or testing) functions [5] used in the MoM's:

$$t_{s'}(y) = \begin{cases} \sin\left\{k\left[h-\left(y+\dfrac{b}{2}\right)\right]\right\}, & s'=1 \\ t_1(y)+\alpha\left(1-\cos\left\{k\left[h-\left(y+\dfrac{b}{2}\right)\right]\right\}\right) & \\ \qquad s'=2 & \end{cases} \tag{3a}$$

and $p_{i'}(\phi')$ is a function defined by

$$p_{i'}(\phi') = \begin{cases} 1, & \phi'_{i'} - \dfrac{\Delta}{2} < \phi'_{i'} < \phi'_{i'} + \dfrac{\Delta}{2} \\ 0, & \text{elsewhere.} \end{cases} \tag{3b}$$

Inside (3), the parameter α is chosen such that the orthogonality condition is satisfied by the testing functions, i.e.,

$$\int_{-b/2}^{-b/2+h} t_1(y)t_2(y)\,dy = 0.$$

Therefore, α may be expressed as

$$\alpha = -\frac{\displaystyle\int_{-b/2}^{-b/2+h} t_1(y)t_1(y)\,dy}{\displaystyle\int_{-b/2}^{-b/2+h} t_1(y)\left(1-\cos\left\{k\left[h-\left(y+\frac{b}{2}\right)\right]\right\}\right)dy}. \tag{4}$$

The electric DGF's for the semi-infinite rectangular waveguide with multiple loads have been formulated earlier in [8] and can be directly used in the computation of the input impedance. To compare with the experimental data, the input impedance of the probe located in a dielectric-loaded rectangular cavity will be computed. Prior to this, the DGF's in each cavity region divided by the dielectric are needed. By reducing the generalized formulas given in [8], the DGF's in each region of the dielectric-loaded cavity are formulated in Appendix A. The rectangular cavity with a single load is formed on the assumption that the last region of a three-layers is a conductor. These DGF's are constructed in terms of the vector–wave functions with the well-known piloting vector $\hat{\boldsymbol{z}}$, and thus are referred to as the conventional form.

The magnetic DGF is also formulated in Appendix A by simplifying the generalized DGF's given in [8]. However, it is not recommended for use in our calculation here. This is because the conventional form of the DGF is not convenient to use. Due to the step-functional change in the $\hat{z}$-direction and a Bessel-functional variation in the $\hat{x}$-direction at the magnetic-source point, the commercially available double integration subroutine has to take these transitions into account and this reduces the computational speed for a given accuracy or introduces errors for a given number of iteration. Evidence of improvement resulting from the use of the alternative form of DGF has been obtained previously by [10] which compared the computational results with the measured input impedance of the probe in a rectangular cavity. The alternative form of the DGF with $\hat{y}$-directed source discontinuity is easier to implement as only the source region of interest $y \geq y'$ is needed. This alternative magnetic DGF has been derived in Appendix B using the discrete eigenvalues of the TE and TM modes and their corresponding eigenfunctions.

C. The Moment Method and Probe-Input Impedance

Once the DGF's are developed, the electric- and magnetic-current distributions can be determined using the boundary conditions over the surface of the conducting metallic probe. Thus, the boundary conditions at N points on the probe surface give:

$$\sum_{i'=1}^{8} \boldsymbol{E}^{J}_{yi,\,i'} + \boldsymbol{E}^{I}_{yi} = 0, \qquad i = 1,\, 2,\, 3,\, 4. \tag{5}$$

Multiplying (5) by the testing equations (i.e., first t_1 and then t_2) and then integrating it throughout the entire length of the probe result in the following matrix equation:

$$\sum_{i'=1}^{4} \sum_{s'=1}^{2} Z_{si,\,s'i'} j_{s'i'} = -\int_{-b/2}^{-b/2+h} t_s(y) E^{I}_{yi}(y)\, dy = V_{si} \tag{6a}$$

or

$$\mathbf{Zj} = \mathbf{V} \tag{6b}$$

where $\mathbf{Z}$ is an 8×8 matrix determined after substitution of (1a) in (5), $\mathbf{j}$ is an 8×1 matrix that consists of elements representing unknown coefficients of the current $J_y(y', \phi)$, and $\mathbf{V}$ is also an 8×1 matrix consisting of the elements V_{si}.

Once the matrix equation is solved, the coefficients of the current distribution and hence the current distribution will be obtained. With the known currents, the input impedance and the reflection coefficients are determined by

$$Z_{\text{in}} = \frac{V_0}{I_{\text{in}}} = \frac{V_0}{\displaystyle\int_0^{2\pi} J_y\left(-\frac{b}{2}, \pi\right) r_i\, d\phi} \tag{7}$$

$$\Gamma = \frac{Z_{\text{in}} - Z_0}{Z_{\text{in}} + Z_0} \tag{8}$$

where Z_0 is the characteristic impedance (50 Ω in the experiment). It is noticed that there are several definitions of the input impedance [1], [5], and [15]—this paper adopted the definition given in [5] and [6].

III. Input Impedance of a Probe in a Dielectric-Loaded Cavity

Following the procedure introduced in the last section, the input impedance can be computed. Prior to this, it is necessary to compute the discrete eigenvalues for TE and TM modes inside the first region. The eigenvalues of the TE and TM modes in the second region can be determined from the characteristic equations in (B-3), but the computation is not so easy and straightforward.

A. Discrete Eigenvalues of TE and TM Modes

To gain an insight into the details, the complete eigenvalues of the TE and TM modes at frequencies of 8.8, 10, and 11.44 GHz in the first region have been obtained. These values are generated using commercially available software MATHEMATICA where the Jacobian method is employed. Care must be exercised because it is easy to miss out or to repeat some of the discrete eigenvalues η_{e1} and η_{o1}. Since these eigenvalues for the given TE and TM modes correspond to the eigenvalue for an empty cavity, $n\pi/c$ has been used to check whether there is any missing eigenvalue. While the *FindRoot* procedure in MATHEMATICA is tabulated for different n values, a proper starting value that varies with the operating frequency and cavity dimension c must be chosen for systematic generation of these eigenvalues.

In the calculation, the dielectric used is Teflon, the relative permittivity ϵ_r of which is a complex quantity and a function of frequency. Therefore, the corresponding value at its respective frequency point must be considered in the computation. The permittivity of the piece of Teflon used has been measured using the dielectric-probe application kit in conjunction with the HP8510 network analyzer.

B. Numerical and Experimental Results

To verify our theoretical analysis, measurements of the input impedance of a coaxial probe-excited loaded cavity have been made. The experimental data of the normalized reactance and the phase of reflection coefficients are shown in Fig. 3(a) and (b) against the frequency f. The cross-section parameters of the rectangular cavity used are: $a = 22.9$ mm and $b = 10.2$ mm. The $\hat{z}$-directional dimensions of the cavity are: $z_0 = -31.9$ mm, $z_1 = 20$ mm, and $z_2 = 25$ mm where the thickness of the dielectric medium is $z_2 - z_1 = 5$ mm. The height, inner radius, and outer radius of the metallic probe are: $h = 8.7$ mm, $r_{\text{in}} = 0.65$ mm and $r_{\text{out}} = 2.05$ mm, respectively. The dielectric used to fill up part of the cavity is Teflon.

The experimental data are also compared with the computed results. The comparison made in Fig. 3(a) and (b) shows reasonably good agreement between theory and experiment,

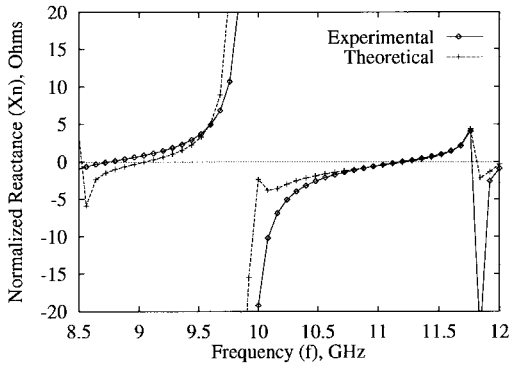

(a)

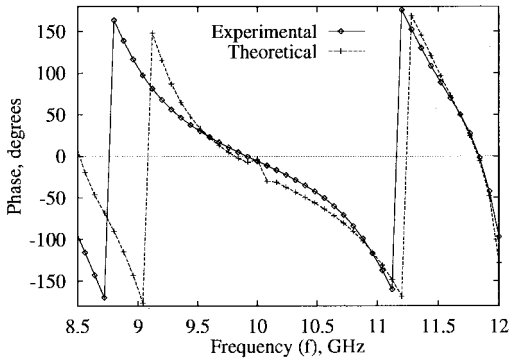

(b)

Fig. 3. Comparison of measured data ("*experimental*" curve) and numerical results ("*theoretical*" curve). (a) Reactance of the probe and (b) phase of reflection coefficient. The thickness $z_2 - z_1$ of the dielectric is 5 mm.

particularly at the frequency of interest ranging from 10 to 12 GHz.

C. Discussions: Numerical Interpolations

As shown in Fig. 3(a) and (b), a kink is found around the frequency of 10 GHz. Detailed debugging checks through the program showed that this kink arises because double integration is poorly converged as well as the ill-condition of the matrix $\mathbf{Z}$ inside the procedure of the MoM's. Similar phenomena were supported by [16]. Such numerical problems have been found near the resonant frequencies. This problem near resonance is due to the creation of an approximate impedance matrix $\mathbf{Z}$, which has the wrong resonant frequency (i.e., it is not consistent with that of the radiation problem). This suggests that the calculated input reactance and the phase-of-reflection coefficient around the frequency of 10 GHz are inaccurate. The $L1$ condition number is used to show the computation errors. Singular value decomposition (SVD) [16] could be used instead of Gaussian elimination to improve the results at the kinks.

With the same parameters used in Fig. 3, the $L1$ condition number of the $\mathbf{Z}$ matrix for the case of the dielectric-loaded rectangular cavity has been plotted in Fig. 4 as a function of frequency. From this figure, the authors can see that the $L1$ number becomes very large around the region of the kinks and that two possible kinks exist, one at about 8.5 GHz and the other at about 10 GHz.

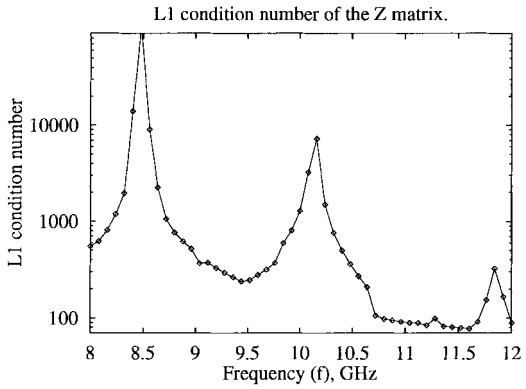

Fig. 4. $L1$ condition number of the fields inside a dielectric-loaded rectangular cavity as a function of frequency. The same parameters of Fig. 4 have been used in the computation.

It is found that when the $\mathbf{Z}$ matrix becomes singular at a particular frequency, the kink occurs around that frequency. Physically, the range around the frequency corresponds to the region where the modes in the rectangular cavity change from the series to the parallel resonance or vice versa. The singularity of the matrix is independent of the form of DGF's used, although the conventional and alternative forms of DGF's affect the elements of $\mathbf{V}$ or the coefficients of $\boldsymbol{E}^{I}_{yi}$. It is also found from the computation that these kinks always exist unless a suitable numerical interpolation is assumed in the procedure of the MoM's. A frequency shift is also found in the phase plot between the experimental and theoretical results. This suggests an electrical delay error in the measurement. Therefore, the extra electrical delay that describes the transfer of the calibration point to the reference plane must be determined accurately.

IV. Conclusion

This paper has presented a full-wave analysis of the input impedance of a coaxial probe located inside a semi-infinite rectangular waveguide with multiple loads. The MoM's together with DGF technique is applied in the analysis. To extend the general analysis to possible applications, a rectangular cavity with a dielectric load excited by the coaxial probe is investigated. While the conventional form of electromagnetic DGF is obtained by reducing the general results given in [8], an alternative form of the magnetic DGF is formulated using the discrete eigenvalues. The input reactance of the probe and the phase-of-reflection coefficient are computed and compared with the measured data. Reasonably good agreement between theory and experiment is found. The authors also computed the results by using the conventional and alternative forms of magnetic DGF's and compared them with the experimental data. It is found from the comparison that a combination of the conventional electric DGF for the electric filamentary source and the alternative form of the magnetic DGF for the magnetic aperture source can provide better accuracy for analyzing a coaxial probe excitation inside a rectangular cavity loaded with a dielectric layer. It is found that kinks exist around certain frequencies when the MoM's matrix $\mathbf{Z}$ becomes singular.

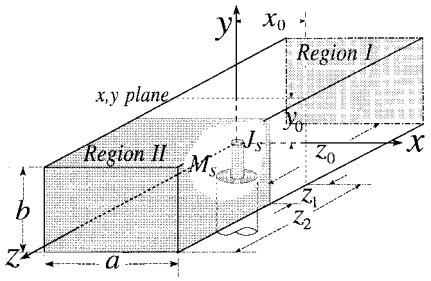

Fig. 5. Geometry of a rectangular loaded cavity.

APPENDIX A
ELECTROMAGNETIC DGF'S FOR A RECTANGULAR LOADED CAVITY

Electric and magnetic types of DGF's for a semi-infinite rectangular waveguide have been developed by [8] and their coefficients have been generally derived. A rectangular cavity with a load shown in Fig. 5 can be considered as a semi-infinite waveguide with a dielectric load and a conducting load. By assuming the third region (in [8]) of the waveguide filled with a perfect conductor (see Fig. 2 for the configuration), the DGF's can be reduced from the general formulas.

A. Representation of DGF's

When a rectangular cavity is filled with a dielectric slab at one end, the space in the cavity is divided into two regions, namely, Region I and Region II. As shown in Fig. 5, the source is located in the first Region I and so is the field point. To simplify the expression, the symbols f (=1 or 2) and s (=1) denote the region numbers of the field and source points, respectively.

The principle of scattering superposition gives the DGF $\overline{\boldsymbol{G}}_{e_m}^{(f1)}(\boldsymbol{r},\boldsymbol{r}')$ which is the sum of the unbounded (with respect to z-direction) dyadic $\overline{\boldsymbol{G}}_{e_m 0}(\boldsymbol{r},\boldsymbol{r}')$ and the scattering DGF $\overline{\boldsymbol{G}}_{e_m S}^{(f1)}(\boldsymbol{r},\boldsymbol{r}')$ contributed by the interfaces perpendicular to the z-direction. In mathematical form, it is

$$\overline{\boldsymbol{G}}_{e_m}^{(f1)}(\boldsymbol{r},\boldsymbol{r}')=\overline{\boldsymbol{G}}_{e_m 0}(\boldsymbol{r},\boldsymbol{r}')\delta_f^1+\overline{\boldsymbol{G}}_{e_m S}^{(f1)}(\boldsymbol{r},\boldsymbol{r}') \tag{A-1}$$

where δ_f^s denotes Kronecker delta.

The unbounded electric and magnetic types of DGF's $\overline{\boldsymbol{G}}_{e_m 0}(\boldsymbol{r},\boldsymbol{r}')$ consisting of the singularity and the principal value is given by

$$\begin{aligned}\overline{\boldsymbol{G}}_{e_m 0}(\boldsymbol{r},\boldsymbol{r}')&=-\frac{\hat{\boldsymbol{z}}\hat{\boldsymbol{z}}\delta(\boldsymbol{r}-\boldsymbol{r}')}{k_0^2}+PV_\delta\overline{\boldsymbol{G}}_{e_m 0}(\boldsymbol{r},\boldsymbol{r}')\\&=-\frac{\hat{\boldsymbol{z}}\hat{\boldsymbol{z}}\delta(\boldsymbol{r}-\boldsymbol{r}')}{k_0^2}+\frac{i}{ab}\sum_{n=0}^{\infty}\sum_{m=0}^{\infty}\frac{2-\delta_0}{\gamma_0 k_c^2}\\&\quad\cdot\begin{cases}\boldsymbol{M}_{\substack{e\\o}mn}(\gamma_0)\boldsymbol{M}'_{\substack{e\\o}mn}(-\gamma_0)\\\quad+\boldsymbol{N}_{\substack{o\\e}mn}(\gamma_0)\boldsymbol{N}'_{\substack{o\\e}mn}(-\gamma_0), & z\ge z'\\ \boldsymbol{M}_{\substack{e\\o}mn}(-\gamma_0)\boldsymbol{M}'_{\substack{e\\o}mn}(\gamma_0)\\\quad+\boldsymbol{N}_{\substack{o\\e}mn}(-\gamma_0)\boldsymbol{N}'_{\substack{o\\e}mn}(\gamma_0), & z<z'\end{cases}\\&\qquad(-\infty<z<\infty;\ -\infty<z'<\infty)\end{aligned} \tag{A-2}$$

where δ_0 (=1 for m or $n=0$, and 0 otherwise) denotes the Kronecker delta and $\gamma_0^2=k_0^2-k_c^2$ and PV_δ represents the principal value.

The scattering DGF $\overline{\boldsymbol{G}}_{e_m S}^{(fs)}(\boldsymbol{r},\boldsymbol{r}')$ can be presented as follows [17] and [18] for the first region,

$$\begin{aligned}\overline{\boldsymbol{G}}_{e_m S}^{(11)}(\boldsymbol{r},\boldsymbol{r}')&=\frac{i}{ab}\sum_{n=0}^{\infty}\sum_{m=0}^{\infty}\frac{2-\delta_0}{\gamma_0 k_c^2}\\&\quad\cdot\{\boldsymbol{M}_{\substack{e\\o}mn}(\gamma_0)[\alpha_{\substack{e\\o}mn}^{(11)\mathrm{TE}}\boldsymbol{M}'_{\substack{e\\o}mn}(\gamma_0)\\&\quad+\beta_{\substack{e\\o}mn}^{(11)\mathrm{TE}}\boldsymbol{M}'_{\substack{e\\o}mn}(-\gamma_0)]\\&\quad+\boldsymbol{N}_{\substack{o\\e}mn}(\gamma_0)[\alpha_{\substack{o\\e}mn}^{(11)\mathrm{TM}}\boldsymbol{N}'_{\substack{o\\e}mn}(\gamma_0)\\&\quad+\beta_{\substack{o\\e}mn}^{(11)\mathrm{TM}}\boldsymbol{N}'_{\substack{o\\e}mn}(-\gamma_0)]\\&\quad+\boldsymbol{M}_{\substack{e\\o}mn}(-\gamma_0)[\alpha_{\substack{e\\o}mn}^{\prime(11)\mathrm{TE}}\boldsymbol{M}'_{\substack{e\\o}mn}(\gamma_0)\\&\quad+\beta_{\substack{e\\o}mn}^{\prime(11)\mathrm{TE}}\boldsymbol{M}'_{\substack{e\\o}mn}(-\gamma_0)]\\&\quad+\boldsymbol{N}_{\substack{o\\e}mn}(-\gamma_0)[\alpha_{\substack{o\\e}mn}^{\prime(11)\mathrm{TM}}\boldsymbol{N}'_{\substack{o\\e}mn}(\gamma_0)\\&\quad+\beta_{\substack{o\\e}mn}^{\prime(11)\mathrm{TM}}\boldsymbol{N}'_{\substack{o\\e}mn}(-\gamma_0)]\},\\&\qquad(z_0<z<z_1;\ z_0<z'<z_1)\end{aligned} \tag{A-3a}$$

and for the second region,

$$\begin{aligned}\overline{\boldsymbol{G}}_{e_m S}^{(21)}(\boldsymbol{r},\boldsymbol{r}')&=\frac{i}{ab}\sum_{n=0}^{\infty}\sum_{m=0}^{\infty}\frac{2-\delta_0}{\gamma_0 k_c^2}\\&\quad\{\boldsymbol{M}_{\substack{e\\o}mn}(\gamma_2)[\alpha_{\substack{e\\o}mn}^{(21)\mathrm{TE}}\boldsymbol{M}'_{\substack{e\\o}mn}(\gamma_0)\\&\quad+\beta_{\substack{e\\o}mn}^{(21)\mathrm{TE}}\boldsymbol{M}'_{\substack{e\\o}mn}(-\gamma_0)]\\&\quad+\boldsymbol{N}_{\substack{o\\e}mn}(\gamma_2)[\alpha_{\substack{o\\e}mn}^{(21)\mathrm{TM}}\boldsymbol{N}'_{\substack{o\\e}mn}(\gamma_0)\\&\quad+\beta_{\substack{o\\e}mn}^{(21)\mathrm{TM}}\boldsymbol{N}'_{\substack{o\\e}mn}(-\gamma_0)]\\&\quad+\boldsymbol{M}_{\substack{e\\o}mn}(-\gamma_2)[\alpha_{\substack{e\\o}mn}^{\prime(21)\mathrm{TE}}\boldsymbol{M}'_{\substack{e\\o}mn}(\gamma_0)\\&\quad+\beta_{\substack{e\\o}mn}^{\prime(21)\mathrm{TE}}\boldsymbol{M}'_{\substack{e\\o}mn}(-\gamma_0)]\\&\quad+\boldsymbol{N}_{\substack{o\\e}mn}(-\gamma_2)[\alpha_{\substack{o\\e}mn}^{\prime(21)\mathrm{TM}}\boldsymbol{N}'_{\substack{o\\e}mn}(\gamma_0)\\&\quad+\beta_{\substack{o\\e}mn}^{\prime(21)\mathrm{TM}}\boldsymbol{N}'_{\substack{o\\e}mn}(-\gamma_0)]\},\\&\qquad(z_1<z<z_2;\ z_0<z'<z_1)\end{aligned} \tag{A-3b}$$

where the symbol N appearing as the superscript and the subscript denotes the region total number of the waveguide. The coordinates z_0, z_1, and z_2 have been shown in Fig. 5. The coefficients $\alpha_{\substack{e\\o}mn}^{(f1)\mathrm{TE,TM}}$, $\beta_{\substack{e\\o}mn}^{(f1)\mathrm{TE,TM}}$, $\alpha_{\substack{e\\o}mn}^{\prime(f1)\mathrm{TE,TM}}$, and $\beta_{\substack{e\\o}mn}^{\prime(f1)\mathrm{TE,TM}}$ are to be determined from the boundary conditions.

B. Scattering Coefficients of DGF's

To simplify the scattering coefficients of the DGF's, the following reflection and transmission coefficients are utilized:

$$\mathcal{R}_{\substack{e\\o}mn}^{f\mathrm{TE}}=\frac{\wp_f\gamma_{f+1}-\wp_{f+1}\gamma_f}{\wp_f\gamma_{f+1}+\wp_{f+1}\gamma_f} \tag{A-4a}$$

$$\mathcal{R}_{\substack{e\\o}mn}^{f\mathrm{TM}}=\frac{\wp_{f+1}\gamma_{f+1}k_f^2-\wp_f\gamma_f k_{f+1}^2}{\wp_{f+1}\gamma_{f+1}k_f^2+\wp_f\gamma_f k_{f+1}^2} \tag{A-4b}$$

$$\mathcal{T}_{\substack{e\\o}mn}^{f\mathrm{TE}} = 1 + \mathcal{R}_{\substack{e\\o}mn}^{f\mathrm{TE}} \tag{A-4c}$$

$$\mathcal{T}_{\substack{e\\o}mn}^{f\mathrm{TM}} = \frac{\wp_f k_{f+1}}{\wp_{f+1} k_f}(1 + \mathcal{R}_{\substack{e\\o}mn}^{f\mathrm{TM}}) \tag{A-4d}$$

where $\wp_f$ $(f = 1, 2, 3)$ denotes the permittivity ϵ_f for the electric type of DGF and the permeability μ_f for the magnetic type of DGF, in the fth region.

According to the formulation given in [8], the general matrices are defined in (A-5) and (A-6) as shown at the bottom of the page, as for the specific case considered, the layer number N is equal to 3, the interface order ℓ is equal to 1 and 2, and the intermediate K is equal to 1. Thus, the intermediate matrix defined in [8] can be written as

$$\mathbf{F}_{\substack{e\\o}mn}^{(1)} = [\mathbf{T}_{\substack{e\\o}mn}^{(2)\mathrm{TE,\,TM}}][\mathbf{T}_{\substack{e\\o}mn}^{(1)\mathrm{TE,\,TM}}] \tag{A-7}$$

where

$$\mathbf{T}_{\substack{e\\o}mn}^{(2)\mathrm{TE,\,TM}} = \frac{1}{\mathcal{T}_{\substack{e\\o}mn}^{2\mathrm{TE,\,TM}}} \cdot \begin{bmatrix} e^{i(\gamma_2-\gamma_3)z_2} & \mathcal{R}_{\substack{e\\o}mn}^{2\mathrm{TE,\,TM}} e^{-i(\gamma_2+\gamma_3)z_2} \\ \mathcal{R}_{\substack{e\\o}mn}^{2\mathrm{TE,\,TM}} e^{i(\gamma_2+\gamma_3)z_2} & e^{-i(\gamma_2-\gamma_3)z_2} \end{bmatrix} \tag{A-8a}$$

$$\mathbf{T}_{\substack{e\\o}mn}^{(1)\mathrm{TE,\,TM}} = \frac{1}{\mathcal{T}_{\substack{e\\o}mn}^{1\mathrm{TE,\,TM}}} \cdot \begin{bmatrix} e^{i(\gamma_1-\gamma_2)z_1} & \mathcal{R}_{\substack{e\\o}mn}^{1\mathrm{TE,\,TM}} e^{-i(\gamma_1+\gamma_2)z_1} \\ \mathcal{R}_{\substack{e\\o}mn}^{1\mathrm{TE,\,TM}} e^{i(\gamma_1+\gamma_2)z_1} & e^{-i(\gamma_1-\gamma_2)z_1} \end{bmatrix}. \tag{A-8b}$$

The element of the matrix $\mathbf{F}_{\substack{e\\o}mn}^{(1)}$ can be expressed as follows:

$$[F_{\substack{e\\o}mn}^{(1)}]_{11} = \frac{1}{\mathcal{T}_{\substack{e\\o}mn}^{1\mathrm{TE,\,TM}} \mathcal{T}_{\substack{e\\o}mn}^{2\mathrm{TE,\,TM}}} [e^{i(\gamma_1-\gamma_2)z_1} \cdot e^{i(\gamma_2-\gamma_3)z_2} + \mathcal{R}_{\substack{e\\o}mn}^{1\mathrm{TE,\,TM}} \mathcal{R}_{\substack{e\\o}mn}^{2\mathrm{TE,\,TM}} \cdot e^{i(\gamma_1+\gamma_2)z_1 - i(\gamma_2+\gamma_3)z_2}] \tag{A-9a}$$

$$[F_{\substack{e\\o}mn}^{(1)}]_{12} = \frac{1}{\mathcal{T}_{\substack{e\\o}mn}^{1\mathrm{TE,\,TM}} \mathcal{T}_{\substack{e\\o}mn}^{2\mathrm{TE,\,TM}}} [\mathcal{R}_{\substack{e\\o}mn}^{1\mathrm{TE,\,TM}} \cdot e^{-i(\gamma_1+\gamma_2)z_1 + i(\gamma_2-\gamma_3)z_2} + \mathcal{R}_{\substack{e\\o}mn}^{2\mathrm{TE,\,TM}} \cdot e^{-i(\gamma_1-\gamma_2)z_1 - i(\gamma_2+\gamma_3)z_2}] \tag{A-9b}$$

$$[F_{\substack{e\\o}mn}^{(1)}]_{21} = \frac{1}{\mathcal{T}_{\substack{e\\o}mn}^{1\mathrm{TE,\,TM}} \mathcal{T}_{\substack{e\\o}mn}^{2\mathrm{TE,\,TM}}} [\mathcal{R}_{\substack{e\\o}mn}^{2\mathrm{TE,\,TM}} \cdot e^{i(\gamma_1-\gamma_2)z_1 + i(\gamma_2+\gamma_3)z_2} + \mathcal{R}_{\substack{e\\o}mn}^{1\mathrm{TE,\,TM}} \cdot e^{i(\gamma_1+\gamma_2)z_1 - i(\gamma_2-\gamma_3)z_2}] \tag{A-9c}$$

$$[F_{\substack{e\\o}mn}^{(1)}]_{22} = \frac{1}{\mathcal{T}_{\substack{e\\o}mn}^{1\mathrm{TE,\,TM}} \mathcal{T}_{\substack{e\\o}mn}^{2\mathrm{TE,\,TM}}} [\mathcal{R}_{\substack{e\\o}mn}^{1\mathrm{TE,\,TM}} \cdot \mathcal{R}_{\substack{e\\o}mn}^{2\mathrm{TE,\,TM}} e^{-i(\gamma_1+\gamma_2)z_1 + i(\gamma_2+\gamma_3)z_2} + e^{-i(\gamma_1-\gamma_2)z_1 - i(\gamma_2-\gamma_3)z_2}]. \tag{A-9d}$$

So far, the intermediates are still valid for a semi-infinite rectangular waveguide with two loads. However, the configuration of interest is a rectangular cavity with a dielectric load, i.e., a semi-infinite rectangular waveguide with a dielectric load (the second region) and a perfectly conducting load (the third region). Thus, we have $\sigma_3 \longrightarrow \infty$, $\varepsilon_3 \longrightarrow i\infty$ so that

$$\mathcal{R}_{\substack{e\\o}mn}^{2\mathrm{TE,\,TM}} = (\pm)(+-)1 \tag{A-10a}$$

$$e^{i\gamma_3 z_2} \longrightarrow 0 \tag{A-10b}$$

$$e^{-i\gamma_3 z_2} \longrightarrow \infty. \tag{A-10c}$$

For the sake of simplicity, we let

$$D^{\mathrm{TE,\,TM}} = e^{-i\gamma_3 z_2} \cdot \mathcal{T}_{\substack{e\\o}mn}^{1\mathrm{TE,\,TM}} \mathcal{T}_{\substack{e\\o}mn}^{2\mathrm{TE,\,TM}} \cdot \{[F_{\substack{e\\o}mn}^{(1)}]_{22} e^{i\gamma_1 z_0} (\mp)(+-)[F_{\substack{e\\o}mn}^{(1)}]_{22} e^{i\gamma_1 z_0}\}. \tag{A-11}$$

Thus, the intermediate $D^{\mathrm{TE,\,TM}}$ reduces to

$$D^{\mathrm{TE,\,TM}} = (\pm)(+-)\mathcal{R}_{\substack{e\\o}mn}^{1\mathrm{TE,\,TM}} e^{-i(\gamma_1+\gamma_2)z_1 + i\gamma_2 z_2 + i\gamma_1 z_0} + e^{-i(\gamma_1-\gamma_2)z_1 - i\gamma_2 z_2 + i\gamma_1 z_0} (\mp)(+-)\mathcal{R}_{\substack{e\\o}mn}^{1\mathrm{TE,\,TM}} \cdot e^{i(\gamma_1+\gamma_2)z_1 - i\gamma_2 z_2 - i\gamma_1 z_0} - e^{i(\gamma_1-\gamma_2)z_1 + i\gamma_2 z_2 - i\gamma_1 z_0} \tag{A-12a}$$

or

$$D^{\mathrm{TE,\,TM}} = 2i\{-\sin[\gamma_1(z_1 - z_0) + \gamma_2(z_2 - z_1)] (\mp)(+-)\mathcal{R}_{\substack{e\\o}mn}^{1\mathrm{TE,\,TM}} \sin[\gamma_1(z_1 - z_0) + \gamma_2(z_1 - z_2)]\}. \tag{A-12b}$$

Finally, the scattering coefficients can be further expressed as

$$\alpha_{\substack{e\\o}mn}^{(11)\mathrm{TE,\,TM}} = [-\mathcal{R}_{\substack{e\\o}mn}^{1\mathrm{TE,\,TM}} e^{i\gamma_2(z_2-z_1)} (\mp)(+-) e^{-i\gamma_2(z_2-z_1)}] \cdot \frac{e^{-i\gamma_1(z_1+z_0)}}{D^{\mathrm{TE,\,TM}}} \tag{A-13a}$$

$$\beta_{\substack{e\\o}mn}^{(11)\mathrm{TE,\,TM}} = [e^{i\gamma_2(z_2-z_1)} (\pm)(+-)\mathcal{R}_{\substack{e\\o}mn}^{1\mathrm{TE,\,TM}} e^{-i\gamma_2(z_2-z_1)}] \cdot \frac{e^{i\gamma_1(z_1-z_0)}}{D^{\mathrm{TE,TM}}} \tag{A-13b}$$

$$\alpha_{\substack{e\\o}mn}^{\prime(11)\mathrm{TE,\,TM}} = \beta_{\substack{e\\o}mn}^{(11)\mathrm{TE,\,TM}} \tag{A-13c}$$

$$\mathbf{F}_{\substack{e\\o}mn}^{(K)} = \begin{Bmatrix} [F_{\substack{e\\o}mn}^{(K)}]_{11} & [F_{\substack{e\\o}mn}^{(K)}]_{12} \\ [F_{\substack{e\\o}mn}^{(K)}]_{21} & [F_{\substack{e\\o}mn}^{(K)}]_{22} \end{Bmatrix} = [\mathbf{T}_{\substack{e\\o}mn}^{(N-1)\mathrm{TE,\,TM}}][\mathbf{T}_{\substack{e\\o}mn}^{(N-2)\mathrm{TE,\,TM}}] \cdots [\mathbf{T}_{\substack{e\\o}mn}^{(K+1)\mathrm{TE,\,TM}}][\mathbf{T}_{\substack{e\\o}mn}^{(K)\mathrm{TE,\,TM}}] \tag{A-5}$$

and

$$\mathbf{T}_{\substack{e\\o}mn}^{(\ell)\mathrm{TE,\,TM}} = \frac{1}{\mathcal{T}_{\substack{e\\o}mn}^{\ell\mathrm{TE,\,TM}}} \begin{bmatrix} e^{i(\gamma_\ell-\gamma_{\ell+1})z_\ell} & \mathcal{R}_{\substack{e\\o}mn}^{\ell\mathrm{TE,\,TM}} e^{-i(\gamma_\ell+\gamma_{\ell+1})z_\ell} \\ \mathcal{R}_{\substack{e\\o}mn}^{\ell\mathrm{TE,\,TM}} e^{i(\gamma_\ell+\gamma_{\ell+1})z_\ell} & e^{-i(\gamma_\ell-\gamma_{\ell+1})z_\ell} \end{bmatrix}. \tag{A-6}$$

$$\beta_{\substack{e\\o}mn}^{\prime(11)\mathrm{TE,\,TM}} = [-\mathcal{R}_{\substack{e\\o}mn}^{1\mathrm{TE,\,TM}} e^{-i\gamma_2(z_2-z_1)}(\mp)(+-)e^{i\gamma_2(z_2-z_1)}] \cdot \frac{e^{i\gamma_1(z_1+z_0)}}{D^{\mathrm{TE,\,TM}}} \tag{A-13d}$$

where $D^{\mathrm{TE,\,TM}}$ is given by (A-12a) or (A-12b). From (A-13c), the symmetry of the DGF with respect to the field and source points is shown.

Appendix B
Alternative Magnetic DGF for a Rectangular Loaded Cavity

A. Magnetic DGF for a Loaded Cavity

Considering a rectangular cavity of two regions ℓ ($\ell = 1, 2$). The principle of separation of variables gives the scalar eigenfunctions of TE (or e mode) and TM (or o mode) modes as follows: for $0 \le z \le d$ or $\ell = 1$,

$$\psi_{\substack{e\\o}mn}(\eta_1) = \begin{matrix}\cos\\ \sin\end{matrix}\left(\frac{m\pi x}{a}\right)\begin{matrix}\cos\\ \sin\end{matrix}\left(\frac{p\pi y}{b}\right)\begin{matrix}\sin\\ \cos\end{matrix}(\eta_1 z) \tag{B-1a}$$

and for $d \le z \le c$ or $\ell = 2$,

$$\psi_{\substack{e\\o}mn}(\eta_2) = \begin{matrix}\cos\\ \sin\end{matrix}\left(\frac{m\pi x}{a}\right)\begin{matrix}\cos\\ \sin\end{matrix}\left(\frac{p\pi y}{b}\right)\begin{matrix}\sin\\ \cos\end{matrix}[\eta_2(c-z)]. \tag{B-1b}$$

The eigenvalues determined by the boundary conditions at the walls $x = 0, a$ and $y = 0, b$ for both TE and TM modes are given by

$$k_x = \frac{m\pi}{a}, \qquad m = 0, 1, 2, \cdots \tag{B-2a}$$

$$k_y = \frac{p\pi}{b}, \qquad p = 0, 1, 2, \cdots. \tag{B-2b}$$

The eigenvalues can be determined from the boundary conditions at the walls $z = 0, c$ and the interface $z = d$ satisfied by the TE (*e*ven) and TM (*o*dd) modes. The conditions can be written in terms of characteristic equations given by

$$\frac{\mu_1}{\eta_{e1}}\tan(\eta_{e1}d) = -\frac{\mu_2}{\eta_{e2}}\tan(\eta_{e2}t) \tag{B-3a}$$

$$\frac{\eta_{o1}}{\epsilon_1}\tan(\eta_{o1}d) = -\frac{\eta_{o2}}{\epsilon_2}\tan(\eta_{o2}t) \tag{B-3b}$$

and the continuity equation of the propagation constant given by

$$k_1^2 - \eta_{\substack{e\\o}1}^2 = k_2^2 - \eta_{\substack{e\\o}2}^2. \tag{B-3c}$$

It is obvious that the eigenvalues are functions of the mode number n. Thus, the vector–wave functions of TE and TM modes can be expressed for region ℓ as follows:

$$\boldsymbol{M}_{\substack{e\\o}mn}[k_{\substack{e\\o}g}^{\ell} y;\, \eta_{\substack{e\\o}\ell} z] = \nabla \times \left[\hat{\boldsymbol{z}}\begin{matrix}\cos\\ \sin\end{matrix}\left(\frac{m\pi x}{a}\right)\begin{matrix}\cos\\ \sin\end{matrix}(k_{\substack{e\\o}g}^{\ell} y)\begin{matrix}\sin\\ \cos\end{matrix}(\eta_{\substack{e\\o}\ell} z)\right] \tag{B-4a}$$

$$\boldsymbol{N}_{\substack{e\\o}mn}[k_{\substack{e\\o}g}^{\ell} y;\, \eta_{\substack{e\\o}\ell} z] = \frac{1}{k_\ell}\nabla \times \nabla \times \left[\hat{\boldsymbol{z}}\begin{matrix}\cos\\ \sin\end{matrix}\left(\frac{m\pi x}{a}\right)\begin{matrix}\cos\\ \sin\end{matrix}(k_{\substack{e\\o}g}^{\ell} y)\begin{matrix}\sin\\ \cos\end{matrix}(\eta_{\substack{e\\o}\ell} z)\right]. \tag{B-4b}$$

Furthermore, the scattering DGF's of the first and second kinds can be represented as

1) for Region I, as $y \ge y'$:

$$\begin{aligned}\overline{\boldsymbol{G}}_{\substack{e\\m}}^{(11)} = &-\sum_{m,n}\frac{(2-\delta_m^0)(2-\delta_n^0)}{ac} \cdot \left\{\frac{1}{C_{\substack{e\\o}}}\boldsymbol{M}_{\substack{e\\o}mn}[k_{\substack{e\\o}g}^1(y-l_2);\, \eta_{\substack{e\\o}1} z] \cdot \boldsymbol{M}'_{\substack{e\\o}mn}[k_{\substack{e\\o}g}^1(y'-l_1);\, \eta_{\substack{e\\o}1} z'] \right.\\ &\left. + \frac{1}{C_{\substack{o\\e}}}\boldsymbol{N}_{\substack{o\\e}mn}[k_{\substack{o\\e}g}^1(y-l_2);\, \eta_{\substack{o\\e}1} z] \cdot \boldsymbol{N}'_{\substack{o\\e}mn}[k_{\substack{o\\e}g}^1(y'-l_1);\, \eta_{\substack{o\\e}1} z']\right\}\end{aligned} \tag{B-5a}$$

and as $y \le y'$:

$$\begin{aligned}\overline{\boldsymbol{G}}_{\substack{e\\m}}^{(11)} = &-\sum_{m,n}\frac{(2-\delta_m^0)(2-\delta_n^0)}{ac} \cdot \left\{\frac{1}{C_{\substack{e\\o}}}\boldsymbol{M}_{\substack{e\\o}mn}[k_{\substack{e\\o}g}^1(y-l_1);\, \eta_{\substack{e\\o}1} z] \cdot \boldsymbol{M}'_{\substack{e\\o}mn}[k_{\substack{e\\o}g}^1(y'-l_2);\, \eta_{\substack{e\\o}1} z'] \right.\\ &\left. + \frac{1}{C_{\substack{o\\e}}}\boldsymbol{N}_{\substack{o\\e}mn}[k_{\substack{o\\e}g}^1(y-l_1);\, \eta_{\substack{o\\e}1} z] \cdot \boldsymbol{N}'_{\substack{o\\e}mn}[k_{\substack{o\\e}g}^1(y'-l_2);\, \eta_{\substack{o\\e}1} z']\right\}\end{aligned} \tag{B-5b}$$

where the eigenvalues $\eta_{\substack{e\\o}1}$ and $\eta_{\substack{e\\o}2}$ are functions of the mode number n, an exact expression has been obtained by summing up the series in terms of the eigenvalues p [19], and the orthogonality of the vector–wave functions have been utilized to obtained the following intermediates:

$$k_{\substack{e\\o}g}^{\ell} = \sqrt{k^2 - \left(\frac{m\pi}{a}\right)^2 - (\eta_{\substack{e\\o}\ell})^2}, \qquad \ell = 1, 2 \tag{B-6a}$$

$$C_{\substack{e\\o}} = \left[\left(\frac{m\pi}{a}\right)^2 + \left(k_{\substack{e\\o}g}^1\right)^2\right]k_{\substack{e\\o}g}^1 \sin\left[k_{\substack{e\\o}g}^1 c\right] \cdot \left[1 - \frac{\sin(2\eta_{\substack{e\\o}1}c)}{2\eta_{\substack{e\\o}1}c}\right] \tag{B-6b}$$

and 2) for Region II, as $y \ge y'$:

$$\begin{aligned}\overline{\boldsymbol{G}}_{\substack{e\\m}}^{(21)} = &-\frac{1}{ac}\sum_{m,n}\frac{(2-\delta_m^0)(2-\delta_n^0)}{ac} \cdot \left\{\frac{\mathcal{T}_{\substack{e\\o}M}}{C_{\substack{e\\o}}}\boldsymbol{M}_{\substack{e\\o}mn}[k_{\substack{e\\o}g}^2(y-l_2);\, \eta_{\substack{e\\o}2}(c-z)] \cdot \boldsymbol{M}'_{\substack{e\\o}mn}[k_{\substack{e\\o}g}^1(y'-l_1);\, \eta_{\substack{e\\o}1} z'] \right.\\ &\left. + \frac{\mathcal{T}_{\substack{o\\e}N}}{C_{\substack{o\\e}}}\boldsymbol{N}_{\substack{o\\e}mn}[k_{\substack{o\\e}g}^2(y-l_2);\, \eta_{\substack{o\\e}2}(c-z)] \cdot \boldsymbol{N}'_{\substack{o\\e}mn}[k_{\substack{o\\e}g}^1(y'-l_1);\, \eta_{\substack{o\\e}1} z']\right\}\end{aligned} \tag{B-7a}$$

and as $y \le y'$:

$$\begin{aligned}\overline{\boldsymbol{G}}_{\substack{e\\m}}^{(21)} = &-\sum_{m,n}\frac{(2-\delta_m^0)(2-\delta_n^0)}{ac}\\ &\cdot\left\{\frac{\mathcal{T}_{\substack{e\\o}M}}{C_{\substack{e\\o}}}\boldsymbol{M}_{\substack{o\\e}mn}[k_{\substack{e\\o}g}^2(y-l_1);\,\eta_{\substack{o\\e}2}(c-z)]\right.\\ &\cdot\boldsymbol{M}'_{\substack{e\\o}mn}[k_{\substack{o\\e}g}^1(y'-l_2);\,\eta_{\substack{e\\o}1}z']\\ &+\frac{\mathcal{T}_{\substack{o\\e}N}}{C_{\substack{o\\e}}}\boldsymbol{N}_{\substack{e\\o}mn}[k_{\substack{o\\e}g}^2(y-l_1);\,\eta_{\substack{e\\o}2}(c-z)]\\ &\left.\cdot\boldsymbol{N}'_{\substack{o\\e}mn}[k_{\substack{e\\o}g}^1(y'-l_2);\,\eta_{\substack{o\\e}1}z']\right\}\end{aligned}\tag{B-7b}$$

where

$$\mathcal{T}_{\substack{e\\o}M} = \frac{\wp_1\begin{matrix}\sin\\\cos\end{matrix}(\eta_{\substack{e\\o}1}d)}{\wp_2\begin{matrix}\sin\\\cos\end{matrix}(\eta_{\substack{e\\o}2}t)}\tag{B-8a}$$

$$\mathcal{T}_{\substack{e\\o}N} = \frac{k_1\begin{matrix}\sin\\\cos\end{matrix}(\eta_{\substack{e\\o}1}d)}{k_2\begin{matrix}\sin\\\cos\end{matrix}(\eta_{\substack{e\\o}2}t)}\tag{B-8b}$$

where

$$\wp = \begin{cases}\mu, & \text{for even mode}\\ \epsilon, & \text{for odd mode.}\end{cases}\tag{B-9}$$

B. Magnetic DGF for an Empty Cavity

Obviously, the above DGF's can be reduced to that for the empty rectangular cavity. In fact, for an empty rectangular cavity, we may assume that $t = 0$ and/or $\epsilon_1 = \epsilon_2$. For both cases, the DGF for Region I reduces to that for the empty cavity, that is, the electromagnetic DGF's, $\overline{\boldsymbol{G}}_{e0}$ and $\overline{\boldsymbol{G}}_{m0}$, for a rectangular cavity can be given for $y \gtrless y'$ by

$$\begin{aligned}\overline{\boldsymbol{G}}_{\substack{e\\m}0} = &-\frac{1}{ac}\sum_{m,n}\frac{(2-\delta_m^0)(2-\delta_n^0)}{\left[k^2-\left(\frac{n\pi}{c}\right)^2\right]k_g\sin[k_g b]}\\ &\cdot\begin{cases}\boldsymbol{M}_{\substack{e\\o}mn}(y-l_2)\boldsymbol{M}'_{\substack{o\\e}mn}(y'-l_1)\\ \quad+\boldsymbol{N}_{\substack{e\\o}mn}(y-l_2)\boldsymbol{N}'_{\substack{o\\e}mn}(y'-l_1)\\ \boldsymbol{M}_{\substack{e\\o}mn}(y-l_1)\boldsymbol{M}'_{\substack{o\\e}mn}(y'-l_2)\\ \quad+\boldsymbol{N}_{\substack{e\\o}mn}(y-l_1)\boldsymbol{N}'_{\substack{o\\e}mn}(y'-l_2)\end{cases}\end{aligned}\tag{B-10}$$

where

$$k_g = \sqrt{k^2-\left[\left(\frac{m\pi}{a}\right)^2+\left(\frac{n\pi}{c}\right)^2\right]}\tag{B-11a}$$

$$\boldsymbol{M}_{\substack{e\\o}mn}(y) = \nabla\times\left[\hat{\boldsymbol{z}}\psi_{\substack{e\\o}mn}\right]\tag{B-11b}$$

$$\boldsymbol{N}_{\substack{e\\o}mn}(y) = \frac{1}{k}\nabla\times\nabla\times\left[\hat{\boldsymbol{z}}\psi_{\substack{e\\o}mn}\right].\tag{B-11c}$$

The vector–wave functions are constructed in terms of the scalar eigenfunctions obtained from the separation of variables and given by

$$\psi_{\substack{e\\o}mn} = \begin{matrix}\cos\\\sin\end{matrix}\left(\frac{m\pi x}{a}\right)\begin{matrix}\cos\\\sin\end{matrix}(k_g y)\begin{matrix}\sin\\\cos\end{matrix}\left(\frac{n\pi z}{c}\right).\tag{B-12}$$

As compared with those in [10] where only magnetic DGF was derived, the representation here includes both electric and magnetic types of DGF's. In [10] there was a typographic error. The correct form of the eigenvalue $\psi'_{\substack{e\\o}mn}(x, y, z)$ in [10] should be the one given in (B-12).

REFERENCES

[1] R. E. Collin, *Field Theory of Guided Waves*, 2nd ed. Piscataway, NJ: IEEE Press, 1991.

[2] M. J. Al-Hakkak, "Experimental investigation of the input-impedance characteristics of an antenna in a rectangular waveguide," *Electron Lett.*, vol. 5, no. 21, pp. 513–514, 1969.

[3] A. G. Williamson and D. V. Otto, "Coaxially fed hollow cylindrical monopole in a rectangular waveguide," *Electron Lett.*, vol. 9, no. 10, pp. 218–220, 1973.

[4] A. G. Williamson, "Analysis and modeling of a coaxial-line/rectangular-waveguide junction," *Proc. Inst. Elect. Eng.*, vol. 129, no. 5, pt. H, pp. 262–270, 1982.

[5] J. M. Jarem, "A multifilament method-of-moments solution for the input impedance of a probe-excited semi-infinite waveguide," *IEEE Trans. Microwave Theory Tech.*, vol. MTT-35, pp. 14–19, 1987.

[6] ——, "A method-of-moments analysis and a finite difference time-domain analysis of a probe-sleeve fed rectangular waveguide cavity," *IEEE Trans. Microwave Theory Tech.*, vol. 39, pp. 444–451, 1991.

[7] J. F. Liang, H. C. Chang, and K. A. Zaki, "Coaxial probe modeling in waveguides and cavities," *IEEE Trans. Microwave Theory Tech.*, vol. 40, pp. 2172–2180, 1992.

[8] L. W. Li, P. S. Kooi, M. S. Leong, T. S. Yeo, and S. L. Ho, "Input impedance of a probe-excited semi-infinite rectangular waveguide with arbitrary multilayered loads: Part I—Dyadic Green's functions," *IEEE Trans. Microwave Theory Tech.*, vol. 43, pt. A, pp. 1559–1566, July 1995.

[9] L. W. Li, M. S. Leong, P. S. Kooi, T. S. Yeo, and S. L. Ho, "Numerical study of magnetic Green dyads of the second kind when used for evaluating input impedance of a probe inside a rectangular cavity," in *Proc. 1995 Asia-Pacific Microwave Conf. (APMC'95), KAIST*, vol. 2. Taejon, Korea, Oct. 10–13, 1995, pp. 679–682.

[10] M. S. Leong, L. W. Li, P. S. Kooi, T. S. Yeo, and S. L. Ho, "Input impedance of a probe antenna located inside a rectangular cavity: Theory and experiment," *IEEE Trans. Microwave Theory Tech.*, vol. 44, pp. 1161–1164, July 1996.

[11] A. G. Williamson and D. V. Otto, "Cylindrical antenna in a rectangular waveguide driven from a coaxial line," *Electron Lett.*, vol. 8, no. 22, pp. 545–547, 1972.

[12] A. G. Williamson, "Coaxially fed hollow probe in a rectangular waveguide," *Proc. Inst. Elect. Eng.*, vol. 132, pt. H, pp. 273–285, 1985.

[13] Y. Leviatan, P. G. Li, A. T. Adams, and J. Perini, "Single-post inductive obstacle in rectangular waveguide," *IEEE Trans. Microwave Theory Tech.*, vol. MTT-31, pp. 806–812, 1983.

[14] Y. Leviatan, D. Shau, and A. T. Adams, "Numerical study of the current distribution on a post in a rectangular waveguide," *IEEE Trans. Microwave Theory Tech.*, vol. MTT-32, pp. 1411–1415, 1984.

[15] W. C. Chew, "Analysis of a probe-fed microstrip disk antenna," *Proc. IEE Microwave Antennas Propagat.* vol. 138, pt. H, pp. 185–191, Apr. 1991.

[16] F. X. Canning, "Singular value decomposition of integral equations of EM and applications to the cavity resonance problem," *IEEE Trans. Antennas Propagat.*, vol. 37, pp. 1156–1163, Sept. 1989.

[17] L. W. Li, P. S. Kooi, M. S. Leong, T. S. Yeo, and S. L. Ho, "On the eigenfunction expansion of dyadic Green's functions in rectangular cavities and waveguides," *IEEE Trans. Microwave Theory Tech.*, vol. 43, pp. 700–702, Mar. 1995.

[18] L. W. Li, P. S. Kooi. M. S. Leong, and T. S. Yeo, "Electromagnetic dyadic Green's function in spherically multilayered media," *IEEE Trans. Microwave Theory Tech.*, vol. 42, pt. A, pp. 2302–2310, Dec. 1994.

[19] _____, "Alternative formulations of electric dyadic Green functions of the first and second kinds for an infinite rectangular waveguide with a load," *Microwave Opt. Tech. Lett.*, vol. 8, no. 2, pp. 98–102, Feb. 1995.

Le-Wei Li (S'91–M'92–SM'96) received the B.Sc. degree in physics from Xuzhou Normal University, Xuzhou, China, in 1984, the M.Eng.Sc. degree from China Research Institute of Radiowave Propagation (CRIRP), Xinxiang, China, in 1987, and the Ph.D. degree in electrical engineering from Monash University, Melbourne, Australia, in 1992.

From 1987 to 1989, he spent two years in the Ionospheric Propagation Laboratory, CRIRP. In 1992, he worked at La Trobe University (jointly with Monash University), Melbourne, Australia, as a Research Fellow. Since November 1992, he has been with the Department of Electrical Engineering, National University of Singapore where he is currently a Senior Lecturer. His research interests include electromagnetic theory, radio wave propagation and scattering in various media, microwave propagation and scattering in tropical environments, microstrip antenna radiation, ionospheric propagation and physics, and the high-frequency (HF) radio propagation associated with over-the-horizon backscatter radar.

Dr. Li was a recipient of the Science and Technology Achievement Awards by the CRIRP and the Henan-Province Association of Science and Technology in 1987 and 1989, respectively, the Best Paper Award from the Chinese Institute of Communications for his paper published in *Journal of China Institute of Communications* in 1990, and the Prize Paper Award from the Chinese Institute of Electronics for his paper published in *Chinese Journal of Radio Science* in 1991. He was selected to receive a Ministerial Award for promoting science and technology development by the Ministry of Electronics Industries, China in 1995, and a Young Scientist Award by URSI in 1996.

Pang-Shyan Kooi (M'75) received the B.Sc. degree in electrical engineering from the National Taiwan University, Taiwan, in 1961, the M.Sc. (Tech) degree in electrical engineering from UMIST, U.K., in 1963, and the D.Phil. degree in engineering science from Oxford University, U.K., in 1970.

Since 1970, he has been with the National University of Singapore, Electrical Engineering Department, Singapore, where he is currently a Professor of Electrical Engineering. His current research interests are microwave, millimeter-wave, and solid-state microwave sources.

Mook-Seng Leong (M'81) received the B.Sc. degree in electrical engineering (with first class honors) and the Ph.D. degree in microwave engineering from the University of London, U.K., in 1968 and 1971, respectively.

He is currently a Professor of Electrical Engineering at the National University of Singapore, Singapore. His main research interests include antenna and waveguide boundary-value problems and semiconductor characterization using the SRP technique.

Dr. Leong is a member of the MIT-based Electromagnetic Academy and a Fellow of the Institution of Electrical Engineers, London. He is also the Chairman of the MTT/AP/EMC joint Chapter, Singapore IEEE Section.

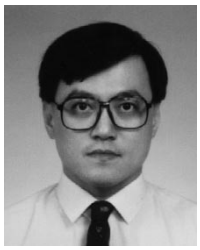

Tat-Soon Yeo (M'80–SM'93) received the B.Eng. (Hons) and M.Eng. degrees in electrical engineering from the National University of Singapore, Singapore, in 1979 and 1981, respectively, and the Ph.D. degree from the University of Canterbury, New Zealand, U.K., in 1985.

Since 1985, he has been with the Electrical Engineering Department of the National University of Singapore where he is currently an Associate Professor. His current research interests are in wave propagation and scattering, antennas, and numerical techniques.

See-Loke Ho received the B.Eng. degree (with first class honors) in 1993 and M.Eng. degree in 1996, both in electrical engineering, from the National University of Singapore, Singapore.

Since 1995, he has been with the National University of Singapore, Center for Wireless Communications, as a Research Engineer. His current research interests are in microwave propagation and scattering, RF circuit designs, and wireless communications.